

Article

Coupling p+n Field-Effect Transistor Circuits for Low Concentration Methane Gas Detection

Xinyuan Zhou ^{1,2}, Liping Yang ¹, Yuzhi Bian ^{1,2}, Xiang Ma ^{1,2}, Ning Han ^{1,3,*}  and Yunfa Chen ^{1,3,*}

¹ State Key Laboratory of Multiphase Complex Systems, Institute of Process Engineering, Chinese Academy of Sciences, Beijing 100190, China; zhouxinyuan14@mails.ucas.edu.cn (X.Z.); yangliping@ipe.ac.cn (L.Y.); bianyuzhi17@mails.ucas.edu.cn (Y.B.); max.nmzx@aliyun.com (X.M.)

² University of Chinese Academy of Sciences, No. 19A Yuquan Road, Beijing 100049, China

³ Center for Excellence in Regional Atmospheric Environment, Institute of Urban Environment, Chinese Academy of Sciences, Xiamen 361021, China

* Correspondence: nhan@ipe.ac.cn (N.H.); chenylf@ipe.ac.cn (Y.C.); Tel.: +86-010-6255-8356

Received: 22 January 2018; Accepted: 19 February 2018; Published: 6 March 2018

Abstract: Nowadays, the detection of low concentration combustible methane gas has attracted great concern. In this paper, a coupling p+n field effect transistor (FET) amplification circuit is designed to detect methane gas. By optimizing the load resistance (R_L), the response to methane of the commercial MP-4 sensor can be magnified ~15 times using this coupling circuit. At the same time, it decreases the limit of detection (LOD) from several hundred ppm to ~10 ppm methane, with the apparent response of 7.0 ± 0.2 and voltage signal of 1.1 ± 0.1 V. This is promising for the detection of trace concentrations of methane gas to avoid an accidental explosion because its lower explosion limit (LEL) is ~5%. The mechanism of this coupling circuit is that the n-type FET firstly generates an output voltage (V_{OUT}) amplification process caused by the gate voltage-induced resistance change of the FET. Then, the p-type FET continues to amplify the signal based on the previous V_{OUT} amplification process.

Keywords: low concentration methane gas; metal oxide gas sensors; field effect transistors; amplification effect

1. Introduction

Methane is a highly flammable and explosive gas widely used in domestic and industrial applications. The lower explosion limit (LEL) of methane is known to be approximately 5% [1,2]. Thus, the trace concentration of methane should be detected fast and reliably in the environment to prevent dangerous explosions. Moreover, in environmental safety, extreme demands are placed on the detection of the potential greenhouse gas methane [3,4]. Recently, various methane sensors have been developed on the basis of catalytic combustion [5–7], metal oxide semiconductor (MOX) [8,9], infrared spectrum [10,11], gas chromatography [12,13], and optical fiber [14,15]. Su et al. reported that the catalytic combustion MEMS (microelectro-mechanical systems) sensors can detect 4000 ppm methane [5]. Shaalan et al. prepared the Co_3O_4 nanoparticles with response (R_a/R_g) of ~1.03 to 2500 ppm methane [8]. The tunable multi-mode diode laser absorption spectroscopy was employed by Gao et al. to respond to 25 ppm methane, with a relative accuracy of 0.27% [11]. There are still challenges in detecting the trace concentration methane. Therein, the MOX gas sensor enjoys a tremendous advantage due to a fast response, chemical stability and low cost [16–18].

Great quantities of new sensing technologies have been developed to improve the gas response of MOX gas sensors and the p+n structure sensor is among them. It consists of two sensitive bodies A and B, where A is a p-type sensing material and B is an n-type sensing material. The theoretical

calculation showed that the sensor realized the multiplication of sensitivity and selectivity when the resistance of B in air is much less than that of A. Wang et al. have developed a p+n combined ethanol sensor to realize the multiplication of selectivity and sensitivity, as compared with the single p-type or n-type gas sensor [19]. However, it has not been widely applied until now, due to a lack of highly sensitive p-type MOX sensors.

In our previous work, an n-type field effect transistor (FET) circuit [20] has been reported to amplify the voltage signal of the MOX gas sensor. For example, this n-type FET circuit is capable of magnifying the response of TGS2602 sensors to toluene by 5–6 times, so that TGS2602 sensors are able to respond effectively to ~ 0.1 ppm toluene, lower than the highest permissible limit (0.26 ppm) of toluene in the indoor air of cars. The amplification effect is because there is a dramatic resistance change of n-FET induced by a tiny change of the gate voltage. However, a new circuit with even larger magnification factors (MF) is expected to improve the gas response of MOX sensors, in order to meet the needs of low concentration dangerous gas detection. In this study, both p-type and n-type FETs have been combined in a circuit to form the coupling p+n FET circuit, in order to detect low concentration methane, on the basis of the commercial sensor MP-4.

2. Design Scheme of the Amplification Circuit

Figure 1 schematically shows the circuit for the methane sensor, which transfers from the traditional circuit to the p-type FET circuit and then to the coupling p+n FET circuit. For the traditional circuit, load resistance (R_L) and MOX gas sensor (R_S) are put in series in the circuit. Then, a bias voltage of 5 V (V_{CC}) is applied and the partial voltage of the R_L is the output voltage (V_{OUT}) signal. Afterwards, select an appropriate R_L to make V_{OUT} as low as ~ 0.4 V in clean air. When R_S makes contact with the target gas, the reduced R_S will lead to the increase of the circuit current and further, V_{OUT} will become larger. Thus, the change of V_{OUT} only depends on the change of R_S .

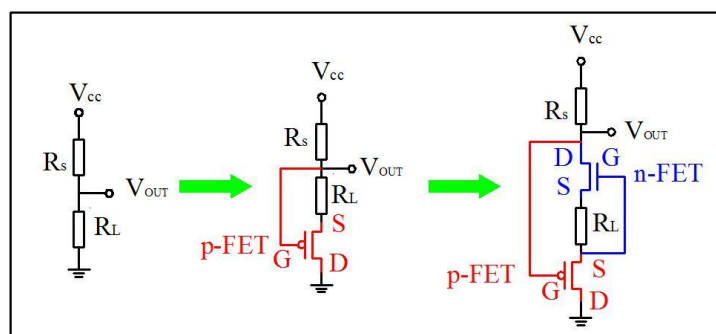


Figure 1. Design scheme of the traditional circuit, the p-type field effect transistor (FET) circuit and the coupling p+n FET circuit for metal oxide semiconductor (MOX) methane sensors.

The p-type FET circuit is different from the traditional circuit, in that a p-type FET is added to the circuit with source (S) connected to R_L and drain (D) grounded. According to the I_D – V_{GS} curve of the p-type FET (seen in Figure S1a), a positive gate source voltage (V_{GS}) is necessary. Therefore, the gate (G) of the p-type FET is connected to the higher potential side of R_L . To make a comparison, the same R_L above is chosen. The baseline of the p-type FET circuit in clean air is similar to that of the traditional circuit because of the negligible resistance of the p-type FET (R_{FET} is $\sim 10^2 \Omega$ in the ON state). Injecting the target gas, R_S will decrease and thus, the circuit current will increase and so does V_{GS} of the p-type FET. V_{GS} shifts positively to let the FET work in the OFF state (R_{FET} is $\sim 10^9 \Omega$), which leads to much larger V_{OUT} . In all, V_{OUT} is under the double influence of R_S and R_{FET} .

Subsequently, an n-type FET is inserted between G and S of the p-type FET forming a coupling p+n FET circuit, as shown in Figure 1. Similarly, V_{OUT} of this coupling circuit in clean air is roughly as low as that of the former two circuits above because both p-type and n-type FETs are in the ON state.

When the target gas is injected, R_S will fall, resulting in the rise of circuit current and the consequently V_{GS} negative shift of n-FET (seen in Figure S1b). Since the resistance of n-FET is more sensitive to the change of V_{GS} (seen in Figure S1c), the negative shift V_{GS} induces the moderate increase of the FET resistance, followed by the V_{DS} growth of n-FET, which is the first V_{OUT} amplification process. Driven by the increasing V_{DS} of n-FET and the partial voltage of R_L , V_{GS} of p-FET shows a clearly positive shift inducing the resistance of p-FET to rise by several orders of magnitude, with the second V_{OUT} amplification process occurring. In brief, the single p-type FET circuit generates the V_{OUT} amplification process only once, while this coupling circuit does twice.

3. Experimental

The methane gas sensors (MP-4) were purchased from the market. The transfer curves ($I_{DS}-V_{GS}$) of typical n-type FETs and p-type FETs are measured by the Keithley 4200 semiconductor analyzer shown in Figure S1, where both 2SK184 and 2SK364 show larger $I_{DS}-V_{GS}$ slopes (the smallest subthreshold swings), when compared with other n-type FETs and so do both 2SJ44 and 2SJ45 FETs. The larger slope makes the FET more sensitive to the gate voltage change, leading to the larger amplification effect according to our previous work [20]. Thus, FETs (2SK184, 2SK364, 2SJ44 and 2SJ45) are utilized to form the coupling p+n FET circuit. All of them are used without any modification. The static gas sensing test system (Hanwei WS-30A, Zhengzhou, China) [21–24] is utilized to study the sensing property of MP-4. The load resistance card is the standard accessory of the system and p-FETs and n-FETs are soldered orderly onto the resistance card with D, S, and G electrodes shown in Figure 1. Inject a different volume of 5% standard methane gas into the gas chamber (total volume 18 L) to generate a different concentration of methane gas, varying from 10 ppm to 150 ppm. R_a and R_g are sensor resistances (R_S) in air and methane gas respectively. Thus, the response of MP-4 to methane is defined as $\text{Response} = R_a/R_g$ [25–27] for the traditional circuit without FET, while the response is defined as $\text{Response} = R_a/R_g \times MF$ for the amplification circuit with FET. The magnification factor (MF) of FET is defined as $MF = (R_L + R_{FET,g})/(R_L + R_{FET,a})$ [20], where $R_{FET,a}$ and $R_{FET,g}$ represent FET resistance in the air and methane gas respectively.

4. Results and Discussion

4.1. Single FET Amplification Circuit

2SJ45 (~0.04 k Ω in the ON state) is adopted in the p-type FET amplification circuit (seen in Figure 1). R_L is set as 1.0, 2.0, and 3.0 k Ω and the typical response curves with and without 2SJ45 FET are shown in Figure 2a and in Figure S3a in the supporting information. Figure 2a shows that the response to 100 ppm methane is about 2, in accordance with that of the manual, although there would be device–device variations and gas concentration variations. Figure 2a also illustrates that 2SJ45 is capable of enhancing the response of the MP-4 sensor to methane from 10 to 100 ppm to varying degrees. The resultant amplifications are shown in Figure 2b by testing at least four sensors, where it is obvious that a maximum MF of ~6.5 is obtained using the 2.0 k Ω resistor. In the meantime, it is noteworthy that every MF of the FET circuit with 2.0 k Ω is larger than that of the FET circuit with 1.0 and 3.0 k Ω because high R_L would result in high $(R_L + R_{FET,a})$, while low R_L would lead to low $(R_L + R_{FET,g})$ leading to low MF of $(R_L + R_{FET,g})/(R_L + R_{FET,a})$ [20].

In our previous work, a single n-type FET amplification circuit with 2SK544 has amplified the signal of three kinds of MOX gas sensors (Figaro TGS2602 sensor for toluene, Hanwei MQ3 sensor for ethanol, Hanwei MP502 sensor for acetone) successfully [20]. In this paper, 2SK364 (~0.05 k Ω in the ON state) is exploited in the n-type FET amplification circuit (seen in Figure S2). Load resistance is set as 0.5, 1.0, and 1.5 k Ω , individually. Figure 3a shows that 2SK364 is able to significantly improve the response of the MP-4 sensor to methane (the corresponding output voltage versus time curves are seen in Figure S3b). Figure 3b illustrates that the magnification effect is maximum when R_L is 1.0 k Ω with the magnification factor up to 7.3. The magnification factor (from 3 to 7.3) depends on the

concentration of methane because different concentrations of methane generate different V_{GS} change of FET, which in turn, leads to different resistance change.

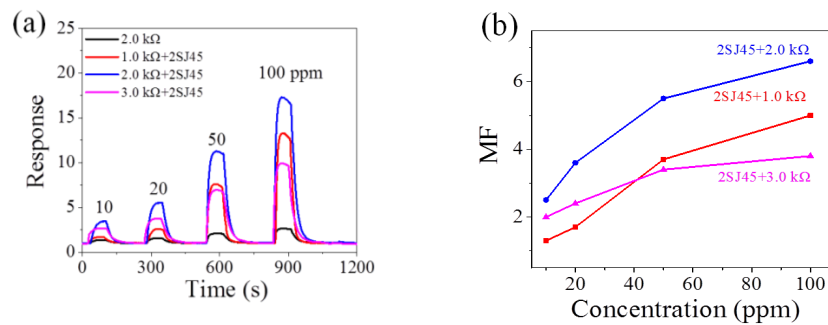


Figure 2. (a) Response of MP-4 to methane from 10 ppm to 100 ppm in the traditional electric circuit and the 2SJ45 FET circuit; (b) magnification factors of the 2SJ45 FET circuit (R_L is 1.0, 2.0 and 3.0 kΩ respectively).

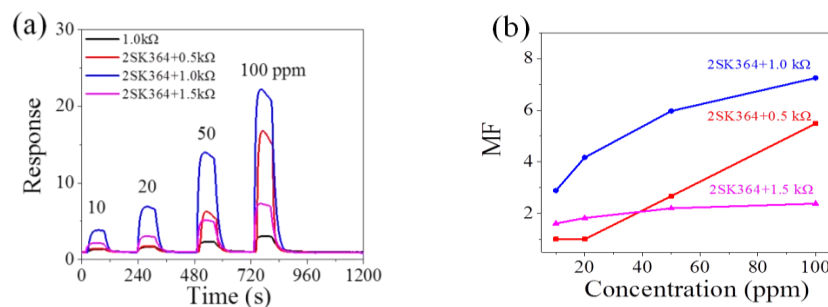


Figure 3. (a) Response of MP-4 to methane from 10 ppm to 100 ppm in the traditional electric circuit and the 2SK364 FET circuit; (b) magnification factors of the 2SK364 FET circuit (R_L is 0.5, 1.0 and 1.5 kΩ respectively).

As mentioned above, the 2SJ45 FET circuit with the 2.0 kΩ resistor and the 2SK364 FET circuit with the 1.0 kΩ resistor are the optimal amplification circuits. They both have different MFs in the same concentration of methane. So, it is essential to quantify their MFs in the given concentration of methane in theory. Thus, the principle of 2SK364 and 2SJ45 enhancing the response of the MP-4 sensor to methane has been further studied. Figure 4 shows the scatter diagrams and exponential function fitting curves of p-type and n-type FET circuits.

For the p-type FET circuit:

$$R_L + R_p = (V_{GS(p)} + V_{DS(p)})/I = 2.19 + 5.39 \times 10^{-17} \exp(147.60 \times I) \quad (1)$$

$$r^2 = 0.999$$

For the n-type FET circuit:

$$R_L + R_n = (V_{GS(n)} + V_{DS(n)})/I = 1.03 + 2.53 \times 10^{-17} \exp(157.42 \times I) \quad (2)$$

$$r^2 = 0.989$$

where R_L is the load resistance; R_p and R_n are the resistances of 2SJ45 and 2SK364 respectively. $V_{GS(p)}$ and $V_{DS(p)}$ are V_{GS} and V_{DS} of 2SJ45 respectively. $V_{GS(n)}$ and $V_{DS(n)}$ are V_{GS} and V_{DS} of 2SK364 respectively. I represents the circuit current.

The black curve and orange solid curve in Figure 4 are expressed respectively as:

$$R_L + R_{FET,air} = V_{CC}/I - R_{S,air} \quad (3)$$

$$R_L + R_{FET,100ppm} = V_{CC}/I - R_{S,100ppm} \quad (4)$$

where V_{CC} is the applied voltage (generally 5 V), $R_{FET,air}$ and $R_{FET,100ppm}$ represent FET resistance in air and 100 ppm methane respectively. $R_{S,air}$ and $R_{S,100ppm}$ are the MP-4 sensor resistance (R_S) in air and in 100 ppm methane individually. $R_{S,air}$ is 20 k Ω and $R_{S,100ppm}$ is 7 k Ω , determined experimentally.

The magnification factor (MF) of the single FET circuit is calculated by Formula (5) [20]:

$$MF = (R_L + R_{FET,100ppm})/(R_L + R_{FET,air}) \quad (5)$$

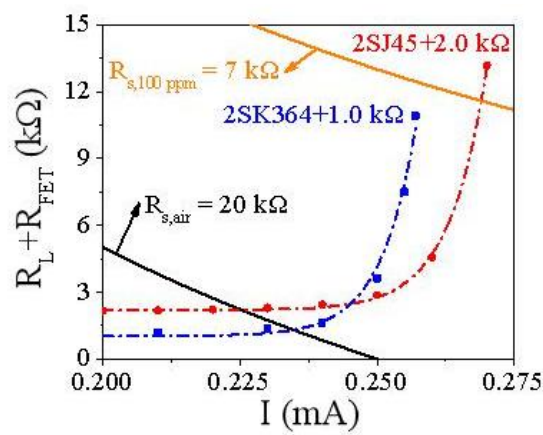


Figure 4. The scatter diagrams and fitting curves of the n-type FET 2SK364 circuit (blue dash curve) and the p-type FET 2SJ45 circuit (red dash curve) with R_L 1.0 and 2.0 k Ω respectively.

For the p-type FET circuit, the value of $R_L + R_{FET,air}$ is the intersection y-coordinate of the Formulas (1) and (3), then $R_L + R_{FET,air}$ is 2.2 k Ω . Similarly, $R_L + R_{FET,100ppm}$ is the intersection y-coordinate of Formulas (1) and (4), then $R_L + R_{FET,100ppm}$ is 11.59 k Ω . Therefore, the theoretical MF is calculated as 11.59 k Ω /2.20 k Ω = 5.3 with the actual MF of 6.5. In the same way, the theoretical MF of n-FET circuit can be calculated. However, Formulas (2) and (3) do not intersect with each other in Figure 4, which means that the amplification effect of n-FET 2SK364 is saturated in 100 ppm methane. Then, $R_L + R_{FET,100ppm}$ is 10.92 k Ω , i.e., the maximum of Formula (2). Finally, the theoretical MF is 10.92 k Ω /1.27 k Ω = 8.6 with the actual MF of 7.3. The theoretical and actual MF s are deemed to be consistent with each other.

4.2. Coupling the p+n FET Amplification Circuit

The experimental results above show that 1.0 k Ω and 2.0 k Ω are the optimal load resistance (R_L) for n-type and p-type FET circuits respectively. Thus, a design scheme is put forward, so that 2SK364 and 2SJ45 are combined in the coupling p+n FET amplification circuit with R_L of 1.0 k Ω , as shown in Figure 1. As mentioned above, when methane is injected into the gas chamber and because 1.0 k Ω is the optimal R_L of 2SK364, not only is the output voltage amplified (the first V_{OUT} amplification process) but also the resistance of 2SK364 rises. Once R_L and 2SK364 resistance exceed 2.0 k Ω , 2SJ45 will realize the second V_{OUT} amplification process. Therefore, this coupling p+n FET amplification circuit is theoretically feasible.

Figure 5a shows the transient V_{OUT} versus time curves (each R_L is 1.0 k Ω). When the MP-4 sensor responds to 10 ppm and 20 ppm methane, it is found that the single 2SJ45 does not significantly enhance V_{OUT} (red line in Figure 5a), while the single 2SK364 (blue line in Figure 5a) obviously does.

The highest V_{OUT} belongs to the coupling p+n FET circuit (magenta line in Figure 5a); however, 2SJ45 in this coupling circuit plays a role in V_{OUT} amplification, induced by the amplification effect of 2SK364. For higher concentrations of methane (≥ 50 ppm), these two FETs simultaneously play an excellent role in enhancing V_{OUT} , as seen in Figure 5a.

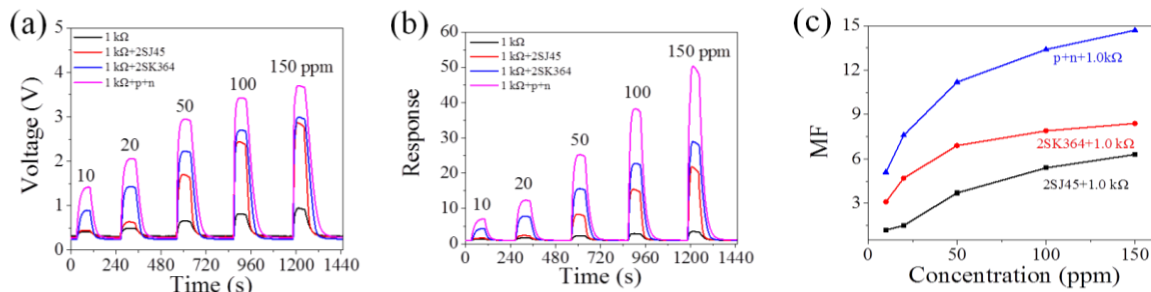


Figure 5. Amplification effect of the coupling p+n FET circuit. Comparison of (a) output voltage and (b) the response among 2SJ45, 2SK364, coupling p+n FET and FET free circuits by connecting a resistor of $R_L = 1.0$ k Ω , and (c) magnification factors comparison among three FET circuits.

Figure 5a,b shows that the MP-4 sensor in the coupling p+n FET circuit responds to 10 ppm with a response of 7.0 ± 0.2 and a voltage change of 1.1 ± 0.1 V, which is high enough to drive an alarmer, preventing the concentration of methane from 5%. At the same time, this coupling circuit extends the LOD of MP-4 from several hundred ppm to 10 ppm. Hence, this coupling circuit enables the MP-4 sensors to effectively detect low concentration methane. In addition, FETs required in this coupling circuit are easy to install and integrate and the cost decreases in bulk production. Figure 5c is the amplification factor versus the concentration curves. It is seen that the amplification factor of the coupling p+n FET circuit is much higher than that of the single FET circuit, with the maximum MF reaching 15. Figure S4 illustrates that the response of the MP-4 gas sensor in this coupling p+n circuit is exponential to the concentration, varying from 10 to 150 ppm, making it convenient to detect methane using this methodology in practical application.

To further prove the universality of this coupling circuit, the p-type FET 2SJ44 and n-type FET 2SK184 are chosen to form a coupling circuit according to Figure 1. This coupling 2SJ44 + 2SK184 circuit also shows an excellent amplification effect. More detailed information is shown in Figure 6.

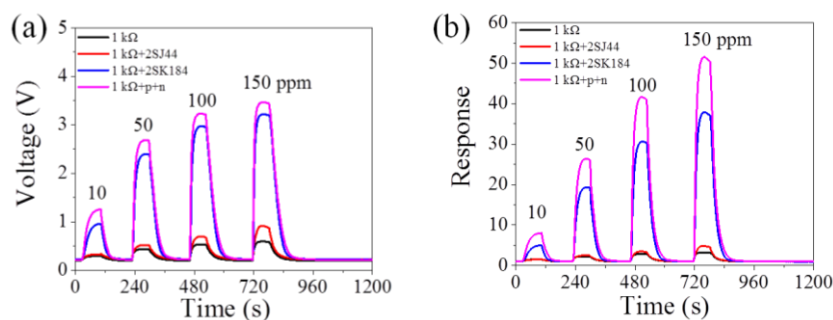


Figure 6. (a) Output voltage and (b) the response among 2SJ44, 2SK184, coupling p+n FET and FET free circuits by connecting a resistor of $R_L = 1.0$ k Ω .

4.3. Mechanism of the Coupling p+n FET Amplification Circuit

The amplification effect of the coupling p+n FET circuit is then studied quantitatively. The blue dashed line in Figure 7 also represents the fitting curve of the n-type FET amplification circuit with 1.0 k Ω . The gray and red dashed lines represent the fitting curves of the p-type FET amplification

circuits with R_L of 1.0 and 2.0 k Ω , respectively. The black and orange solid curves in Figure 7 are similar to those in Figure 4. $R_{S,air}$ is 20 k Ω and $R_{S,150\text{ ppm}}$ is 5.5 k Ω , determined experimentally. For the green line, $R_{S,6.9\text{ ppm}}$ is 18 k Ω , determined theoretically, as shown in Figure S5.

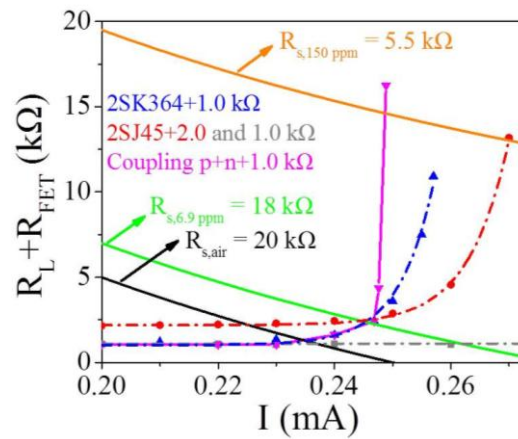


Figure 7. The approximate curve of the coupling p+n FET circuit with R_L of 1.0 k Ω (magenta solid line). The scatter diagrams and fitting curves of the n-type FET 2SK364 circuit with R_L 1.0 k Ω (blue dash curve) and p-type FET 2SJ45 circuits with R_L 1.0 and 2.0 k Ω respectively (gray and red dashed lines).

According to the coupling p+n FET circuit in Figure 1 and Ohmic Law, the following formula can be obtained:

$$V_{GS(p)} = V_{GS(n)} + V_{DS(n)}, \quad (6)$$

$$V_{OUT} = V_{GS(p)} + V_{DS(p)}, \quad (7)$$

$$R_L + R_{FET} = V_{OUT}/I, \quad (8)$$

The formula of the working curve of the coupling p+n FET circuit can be obtained from Formulas (6–8).

$$R_L + R_{FET} = (V_{GS(n)} + V_{DS(n)})/I + V_{DS(p)}/I, \quad (9)$$

$(V_{GS(n)} + V_{DS(n)})/I$ in Formula (9) is exactly the Formula (2) of the n-type FET circuit, reflecting the magnification effect of 2SK364. Meanwhile, $V_{DS(p)}/I$ in Formula (9) is only a part of Formula (1) of the p-type FET circuit. The $V_{DS(p)}$ is difficult to analyze because it is under the double effect of V_{GS} of the two FETs. That is to say, the amplification effect of FET 2J45 is dependent on FET 2SK364. Therefore, the measurement of the working curve of the coupling p+n FET circuit needs to be simplified, approximated, and estimated, and can be divided into three stages:

- The first stage is in clean air, i.e., the baseline of the sensor. The R_L of the coupling p+n FET circuit is 1.0 k Ω . Both of the FETs are in the ON state, so their resistances can be neglected. Therefore, the coupling circuit in clean air is equivalent to the single n-type or p-type FET circuit. Hence, the curves of both the coupling circuit (magenta solid line) and the single n- and p-type FET circuits (blue and gray dash lines) overlap each other, where $R_L + R_{FET} \approx V_{GS(n)}/I = 1.0$ k Ω , as seen in Figure 7.
- When trace concentrations (≤ 6.9 ppm) of methane gas are injected, which is the second stage, 2SK364 starts to enter the OFF state and amplifies V_{OUT} , while 2SJ45 is still in the ON state. Therefore, the coupling p+n FET circuit is equivalent to the single n-type FET circuit, namely $R_L + R_{FET} = (V_{GS(n)} + V_{DS(n)})/I$, whose curve overlaps the fitting curve of the single n-type FET circuit with R_L of 1.0 k Ω (blue dash curve), as shown in Figure 7. It should be noted that all circuits, with or without FETs, cannot effectively detect methane lower than 6.9 ppm if the effective voltage signal is set to 1.0 V.

- Injecting more than 6.9 ppm of methane gas is the third stage. Both 2SK364 and 2SJ45 play an excellent amplifying role. In this stage, the coupling p+n FET circuit is roughly thought of as the single p-type FET circuit, where R_L is subject to the n-FET. Consequently, this coupling circuit can be regarded as the p-type FET circuit with variable R_L , which is distinguished from constant R_L in the former single FET circuit and gives far higher MF than single FET circuits.

The p-type FET circuit with variable R_L is then emphasized. The experimental results show that 2.0 k Ω is the optimal R_L . Hence, 2.0 k Ω is set as the initial resistance. The fitting curves of the p-type FET circuit with constant R_L of 2.1, 2.2 and 2.3 k Ω are shown in Figure S6. The selection of working points of the p-type FET circuit with variable R_L follows two requirements. One is that the point is obviously higher than the fitting curve of the n-type FET circuit (Formula (2)), as seen in Figure 7 to display the amplification role of $V_{DS(p)}/I$, i.e., FET 2SJ45. The other is that the current of the selected point increases rather than decreases. According to these two requirements, the working curve of the coupling p+n FET circuit in the third stage is roughly estimated, which increases almost vertically, as seen in Figure 7. This is the basic reason why the coupling circuit is capable of amplifying the V_{OUT} strikingly.

The working curve of this coupling p+n FET circuit is the magenta solid curve in Figure 7. It reveals the principle of this coupling circuit, that the n-FET firstly generates a V_{OUT} amplification process and then p-FET continues based on the pre-amplification process, where V_{OUT} amplification is derived from the gate voltage inducing resistance change of the FET. It is noteworthy that the estimated curve of this coupling circuit is not the simple superposition of two fitting curves of the p-type and the n-type FET circuits, but rather, a more complex combination. According to Figure 7, the theoretical magnification factor (MF) is calculated as 14.61 k Ω /1.07 k Ω = 13.7, which is the actual MF of 15 in Figure 5c. This indirectly proves the reliability of the estimated curve of the coupling p+n FET circuit.

Moreover, it is also noted that the response time of 15–18 s is not affected by the FETs and neither is the recovery time, as shown in Table S1. Finally, this methodology can also be adopted to detect other gases, as the amplification depends only on the FETs, not on the gases. This is similar to the n-type 2SK544 FET circuit, which is able to amplify the signal of the commercial toluene, ethanol, and acetone MOX gas sensors [20].

For contrast, 2SJ45 and 2SK364 are combined in a circuit forming the former synergetic p+n FET circuit [28] in Figure S7. Obviously, the gate of the p-FET is not connected to the drain of the n-FET but the higher potential side of R_L , which distinguishes the synergetic circuit from the coupling circuit. It should be noted that the p-type and the n-type FETs in this synergetic circuit can work independently. Accordingly, the working curve of the synergetic p+n FET circuit is expressed as below:

$$R_L + R_{FET} = (V_{GS(n)} + V_{DS(n)})/I + (V_{GS(p)} + V_{DS(p)})/I - 1 \text{ k}\Omega, \quad (10)$$

Apparently, the curve of this synergetic circuit shown in Figure S8 is the simple superposition of two working curves of the p-type and n-type FET circuits. Figure S8 also illustrates that the synergetic 2SJ45 + 2SK364 circuit has a similar working curve with a single 2SK364 circuit. Thus, it is theoretically infeasible to combine 2SJ45 and 2SK364 in this synergetic p+n FET circuit.

5. Conclusions

In this paper, a novel coupling FET circuit is designed to detect low concentrations methane. The commercial sensor (MP-4) used in this coupling circuit has shown a response of 7.0 ± 0.2 to 10 ppm methane. Further, the limit of detection decreases from several hundred ppm to 10 ppm, extended by an order of magnitude. It is expected that the monitoring of methane leakage and the early warning of methane explosions will be achieved. At the same time, this coupling FET circuit can amplify the response to methane by 15 times, with the response time and recovery time unaffected by FETs. More importantly, FETs used in this coupling circuit are easy to install, integrate, and the cost increases by only ~10% of the sensor by adding two FETs. The mechanism of this coupling circuit is that the n-FET

firstly generates an output voltage (V_{OUT}) amplification process, caused by the gate voltage-induced resistance change of the FET. Then, the p-FET continues based on the previous V_{OUT} amplification process. It is a more complex combination rather than the simple superposition of two fitting curves of p-type and n-type FET circuits. Finally, this coupling circuit is also promising in other kinds of MOX sensors to detect low concentrations of the target gases.

Supplementary Materials: The following are available online at www.mdpi.com/1424-8220/18/3/787/s1, Figure S1: (a) $I_{DS}-V_{GS}$ curve of four p-type FETs. (b) $I_{DS}-V_{GS}$ curve of four n-type FETs. (c) $dR_{DS}/dV_{GS}-V_{GS}$ curve of 2SJ45 (red) and 2SK364 (blue), Figure S2: Design scheme of the conventional electric circuit, designed single n-type FET amplification circuit for MOX methane sensors, Figure S3: (a) Output voltage of MP-4 to methane from 10 to 100 ppm in the traditional electric circuit and the 2SK364 FET circuit (R_L is 0.5, 1.0 and 1.5 k Ω respectively). (b) Output voltage of MP-4 to methane from 10 ppm to 100 ppm in the traditional electric circuit and the 2SJ45 FET circuit (R_L is 1.0, 2.0 and 3.0 k Ω respectively), Figure S5: Linear fitting line of response of MP-4 versus methane concentration from 10 to 50 ppm in the traditional electric circuit with R_L of 1.0 k Ω (Linear fitting line is $Res = 1.00 + 0.016c$, $r^2 = 0.9996$), Figure S6: The approximate curve of the coupling p+n FET circuit with R_L 1.0 k Ω (magenta solid curve). The scatter diagrams and fitting curves of the n-type FET 2SK364 circuit with R_L 1.0 k Ω (blue dash curve) and p-type FET 2SJ45 circuits with R_L 1.0, 2.0, 2.1, 2.2 and 2.3 k Ω respectively, Figure S7: Design scheme of the synergetic p+n amplification circuit for the MOX methane gas sensor, Figure S8: The working curve of the synergetic p-type 2SJ45 and n-type 2SK364 circuit with R_L of 1.0 k Ω , Table S1: The response time of gas sensor in different circuits with or without FET.

Acknowledgments: This research was financially supported by the National Key R&D Program of China (2016YFC0207100), the National Natural Science Foundation of China (51272253), Guangdong Innovative and Entrepreneurial Research Team Program (No. 2014ZT05C146), and the State Key Laboratory of Multiphase Complex Systems (MPCS-2014-C-01).

Author Contributions: This paper was prepared through a collective effort of all the authors. Xinyuan Zhou proposed the idea, processed data and wrote the paper. Yuzhi Bian performed the experiments. Ning Han, Liping Yang and Xiang Ma contributed the analysis of the results. Ning Han contributed the final revision of this paper. Ning Han and Yunfa Chen directed the research as the principal investigator (PI) of the project.

Conflicts of Interest: The authors declare no conflict of interest.

References

- De Smedt, G.; de Corte, F.; Notele, R.; Berghmans, J. Comparison of two standard test methods for determining explosion limits of gases at atmospheric conditions. *J. Hazard. Mater.* **1999**, *A70*, 105–113. [[CrossRef](#)]
- Vuong, N.M.; Hieu, N.M.; Hieu, H.N.; Yi, H.; Kim, D.; Han, Y.; Kim, M. Ni₂O₃-decorated SnO₂ particulate films for methane gas sensors. *Sens. Actuators B Chem.* **2014**, *192*, 327–333. [[CrossRef](#)]
- Patsha, A.; Sahoo, P.; Amirthapandian, S.; Prasad, A.K.; Das, A.; Tyagi, A.K.; Cotta, M.A.; Dhara, S. Localized Charge Transfer Process and Surface Band Bending in Methane Sensing by GaN Nanowires. *J. Phys. Chem. C* **2015**, *119*, 21251–21260. [[CrossRef](#)]
- Yvon-Durocher, G.; Allen, A.P.; Bastviken, D.; Conrad, R.; Gudasz, C.; St-Pierre, A.; Thanh-Duc, N.; del Giorgio, P.A. Methane fluxes show consistent temperature dependence across microbial to ecosystem scales. *Nature* **2014**, *507*, 488–491. [[CrossRef](#)] [[PubMed](#)]
- Su, J.; Cao, L.; Li, L.; Wei, J.; Li, G.; Yuan, Y. Highly sensitive methane catalytic combustion micro-sensor based on mesoporous structure and nano-catalyst. *Nanoscale* **2013**, *5*, 9720–9725. [[CrossRef](#)] [[PubMed](#)]
- Nagai, D.; Nishibori, M.; Itoh, T.; Kawabe, T.; Sato, K.; Shin, W. Ppm level methane detection using micro-thermoelectric gas sensors with Pd/Al₂O₃ combustion catalyst films. *Sens. Actuators B Chem.* **2015**, *206*, 488–494. [[CrossRef](#)]
- Ercolino, G.; Karimi, S.; Stelmachowski, P.; Specchia, S. Catalytic combustion of residual methane on alumina monoliths and open cell foams coated with Pd/Co₃O₄. *Chem. Eng. J.* **2017**, *326*, 339–349. [[CrossRef](#)]
- Shalan, N.M.; Rashad, M.; Moharram, A.H.; Abdel-Rahim, M.A. Promising methane gas sensor synthesized by microwave-assisted Co₃O₄ nanoparticles. *Mater. Sci. Semicond. Process.* **2016**, *46*, 1–5. [[CrossRef](#)]
- Hussain, T.; Kaewmaraya, T.; Khan, M.; Chakraborty, S.; Islam, M.S.; Amornkitbamrung, V.; Ahuja, R. Improved sensing characteristics of methane over ZnO nano sheets upon implanting defects and foreign atoms substitution. *Nanotechnology* **2017**, *28*, 415502. [[CrossRef](#)] [[PubMed](#)]

10. Gustafsson, U.; Sandsten, J.; Svanberg, S. Simultaneous detection of methane, oxygen and water vapour utilising near-infrared diode lasers in conjunction with difference-frequency generation. *Appl. Phys. B* **2000**, *71*, 853–857. [[CrossRef](#)]
11. Gao, Q.; Zhang, Y.; Yu, J.; Wu, S.; Zhang, Z.; Zheng, F.; Lou, X.; Guo, W. Tunable multi-mode diode laser absorption spectroscopy for methane detection. *Sens. Actuators A Phys.* **2013**, *199*, 106–110. [[CrossRef](#)]
12. Lofffield, N.; Flessa, H.; Augustin, J.; Beese, F. Automated Gas Chromatographic System for Rapid Analysis of the Atmospheric Trace Gases Methane, Carbon Dioxide, and Nitrous Oxide. *J. Environ. Qual.* **1997**, *26*, 560–564. [[CrossRef](#)]
13. Kamiński, M.; Kartanowicz, R.; Jastrzębski, D.; Kamiński, M.M. Determination of carbon monoxide, methane and carbon dioxide in refinery hydrogen gases and air by gas chromatography. *J. Chromatogr. A* **2003**, *989*, 277–283. [[CrossRef](#)]
14. Benounis, M.; Jaffrezic-Renault, N.; Dutasta, J.P.; Cherif, K.; Abdelghani, A. Study of a new evanescent wave optical fibre sensor for methane detection based on cryptophane molecules. *Sens. Actuators B Chem.* **2005**, *107*, 32–39. [[CrossRef](#)]
15. Tao, C.; Li, X.; Yang, J.; Shi, Y. Optical fiber sensing element based on luminescence quenching of silica nanowires modified with cryptophane-A for the detection of methane. *Sens. Actuators B Chem.* **2011**, *156*, 553–558. [[CrossRef](#)]
16. Basu, S.; Basu, P.K. Nanocrystalline Metal Oxides for Methane Sensors: Role of Noble Metals. *J. Sens.* **2009**, *2009*, 1–20. [[CrossRef](#)]
17. Haridas, D.; Gupta, V. Enhanced response characteristics of SnO₂ thin film based sensors loaded with Pd clusters for methane detection. *Sens. Actuators B Chem.* **2012**, *166–167*, 156–164. [[CrossRef](#)]
18. Kim, H.R.; Haensch, A.; Kim, I.D.; Barsan, N.; Weimar, U.; Lee, J.H. The Role of NiO Doping in Reducing the Impact of Humidity on the Performance of SnO₂-Based Gas Sensors: Synthesis Strategies, and Phenomenological and Spectroscopic Studies. *Adv. Funct. Mater.* **2011**, *21*, 4456–4463. [[CrossRef](#)]
19. Wang, Y.; Wu, X.; Zhou, Z. Novel high sensitivity and selectivity semiconductor gas sensor based on the p+n combined structure. *Solid-State Electron.* **2000**, *44*, 1603–1607. [[CrossRef](#)]
20. Zhou, X.; Wang, Y.; Wang, J.; Xie, Z.; Wu, X.; Han, N.; Chen, Y. Amplifying the Signal of Metal Oxide Gas Sensors for Low Concentration Gas Detection. *IEEE Sens. J.* **2017**, *17*, 2841–2847. [[CrossRef](#)]
21. Xing, R.Q.; Xu, L.; Song, J.; Zhou, C.Y.; Li, Q.L.; Liu, D.L.; Song, H.W. Preparation and Gas Sensing Properties of In₂O₃/Au Nanorods for Detection of Volatile Organic Compounds in Exhaled Breath. *Sci. Rep.* **2015**, *5*, 10717. [[CrossRef](#)] [[PubMed](#)]
22. Guan, Y.; Wang, D.W.; Zhou, X.; Sun, P.; Wang, H.Y.; Ma, J.; Lu, G.Y. Hydrothermal preparation and gas sensing properties of Zn-doped SnO₂ hierarchical architectures. *Sens. Actuators B Chem.* **2014**, *191*, 45–52. [[CrossRef](#)]
23. Bai, S.L.; Du, L.; Sun, J.H.; Luo, R.X.; Li, D.Q.; Chen, A.F.; Liu, C.C. Preparation of reduced graphene oxide/Co₃O₄ composites and sensing performance to toluene at low temperature. *RSC Adv.* **2016**, *6*, 60109–60116. [[CrossRef](#)]
24. Qin, N.; Wang, X.H.; Xiang, Q.; Xu, J.Q. A biomimetic nest-like ZnO: Controllable synthesis and enhanced ethanol response. *Sens. Actuators B Chem.* **2014**, *191*, 770–778. [[CrossRef](#)]
25. Chen, A.; Bai, S.; Shi, B.; Liu, Z.; Li, D.; Liu, C.C. Methane gas-sensing and catalytic oxidation activity of SnO₂-In₂O₃ nanocomposites incorporating TiO₂. *Sens. Actuators B Chem.* **2008**, *135*, 7–12. [[CrossRef](#)]
26. Malyshev, V.V.; Pisyakov, A.V. Metal oxide semiconductors based on tin dioxide: Gas-sensitivity to methane in a wide range of temperatures, concentrations and humidities of the gas phase. *J. Anal. Chem.* **2009**, *64*, 90–100. [[CrossRef](#)]
27. Zhang, H.; Cen, Y.; Du, Y.; Ruan, S. Enhanced Acetone Sensing Characteristics of ZnO/Graphene Composites. *Sensors* **2016**, *16*, 1876. [[CrossRef](#)] [[PubMed](#)]
28. Zhou, X.; Wang, Y.; Wang, Z.; Yang, L.; Wu, X.; Han, N.; Chen, Y. Synergetic p+n field-effect transistor circuits for ppb-level xylene detection. *IEEE Sens. J.* **2018**. under review.

